BNL-114004-2017-JA

File # 94984

Emergent optical phononic modes upon nanoscale mesogenic phase transitions

D. Bolmatov, M. Zhernenkov, L. Sharpnack, D. M. Agra-Kooijman, S. Kumar, A. Suvorov, R. Pindak, Y. Q. Cai, and A. Cunsolo

Submitted to: Nano Letters

May 26, 2017

Photon Sciences Department

Brookhaven National Laboratory

U.S. Department of Energy
USDOE Office of Science (SC),
Basic Energy Sciences (BES) (SC-22)

DISCLAIMER

Emergent optical phononic modes upon nanoscale mesogenic phase transitions

Dima Bolmatov,[*,†] Mikhail Zhernenkov,[†] Lewis Sharpnack,[‡] Deña M. Agra-Kooijman,[‡] Satyendra Kumar,[‡] Alexey Suvorov,[†] Ronald Pindak,[†] Yong Q. Cai,[†] and Alessandro Cunsolo[†]

National Synchrotron Light Source II, Brookhaven National Laboratory, Upton, NY 11973, USA, Department of Physics, Kent State University, Kent, Ohio 44242, USA, and Division of Research and Department of Physics, University at Albany, Albany, NY 12222, USA

E-mail: d.bolmatov@gmail.com

Abstract

The investigation of phononic collective excitations in soft matter systems at the molecular scale has always been challenging due to limitations of experimental techniques in resolving low-energy modes. Recent advances in Inelastic X-ray Scattering (IXS) enabled the study of such systems with unprecedented spectral contrast at meV excitation energies. In particular, it has become possible to shed light on the low-energy collective motions in materials whose morphology and phase behavior can easily be manipulated, such as mesogenic systems. The understanding of collective mode behavior with a Q-dependence is the key to implement heat management based on the control of a sample structure. The latter has great potential for a large number of energy-inspired

[*]To whom correspondence should be addressed
[†]National Synchrotron Light Source II, Brookhaven National Laboratory, Upton, NY 11973, USA
[‡]Department of Physics, Kent State University, Kent, Ohio 44242, USA
[¶]Division of Research and Department of Physics, University at Albany, Albany, NY 12222, USA

innovations. As a first step towards this goal, we carried out high contrast IXS measurements on a liquid crystal sample, D7AOB, which exhibits solid-like dynamic features, such as the coexistence of longitudinal and transverse phononic modes. For the first time, we found that these terahertz phononic excitations persist in the crystal, smectic A and isotropic phases. Furthermore, the intermediate smectic A phase is shown to support a van der Waals-mediated non-hydrodynamic mode with an optical-like phononic behavior. The tunability of the collective excitations at nanometer-terahertz scales via selection of the sample mesogenic phase represents a new opportunity to manipulate optomechanical properties of soft metamaterials.

Keywords

nano-acoustics, mesogen dynamics, optical phonons, THz light-phonon coupling, acoustic phononic gaps, soft metamaterials

Phonons, quantized vibrational energies of atoms and molecules, are responsible for the transmission of sound and heat in a preferred direction. Understanding and controlling the phononic properties of materials provide opportunities to thermally insulate buildings, reduce environmental noise and transform waste heat into electricity. At the same time, the local nanoscale structure controls the intermolecular couplings making it possible to manipulate heat and energy transfer with high precision.[1] Such complex microscopic interactions, in particular, when associated with internal hetero-interfaces, controls the macroscopic properties and performance of many complex materials. They lend themselves to applications as optical cooling, light and heat harvesting, and management of thermal conductivity.[1] In recent years, the search for these non-trivial acoustic and non-hydrodynamic effects in the spectrum of density fluctuations in various condensed matter systems has attracted growing attention.[2–12] This spectrum can be directly probed by inelastic scattering measurements, whereby density fluctuations are generated by the collision between a probe particle and the target sample. At infinitesimally low-Q and ω the hydrodynamic theory provides a consistent

account of the dynamic response, resulting from an average over continuous distances and many microscopic interactions.[13] At the molecular level, the hydrodynamic description may not be justified. Nonetheless, for liquids and dense fluids valid arguments can still be invoked in support of hydrodynamic-like behavior of the nanometer-THz spectrum.[14] In fact, these systems are so densely packed that the only short time single particle movements permitted are essentially very rapid in-cage rattling oscillations. This implies that at these short time scales a liquid exhibits a solid-like dynamic response.[15] Consequently, even at the nanometer length and picosecond time scales probed by inelastic x-ray (IXS) and neutron (INS) scattering the dynamic behavior is still averaged over many local interactions (cage collisions) as, in principle, required for a suitably generalized hydrodynamic theory to be valid.[16,17] In binary fluids, this behavior is strongly coupled with microscopic degrees of freedom where short-time kinetic processes become responsible for optical-like phonon excitations whose lifetime remains finite upon approaching macroscopic scales.[17] These excitations are expected to emerge whenever the considered scale matches some characteristic inhomogeneity of the system. They are primarily responsible for interaction with light, thus, providing a broad range of optomechanical applications, as long as the sound-light coupling can be tuned. Therefore, simple liquids, being invariant for both translations and rotations, do not seem ideally suited to observe the onset of non-hydrodynamic modes. In principle, hybrid or partially ordered soft matter systems, such as colloids, diblock copolymers, lyotropic or thermotropic liquid crystals, should be better candidates in which a breach in homogeneity or isotropy occurs at some intermediate distances.

In this paper, we report on combined IXS and X-ray diffraction measurements on a symmetric, weakly polar liquid crystal compound 4,4'-diheptylazoxybenzene (D7AOB) in the crystal (Cryst), smectic *A* (SmA) and isotropic (Iso) phases. The molecules of D7AOB are composed of a rigid azoxybenzene central part and flexible alkyl tails with the phase sequence: Cryst-32^{o}C-SmA-53^{o}C-N-70^{o}C-Iso, where N stands for the nematic phase.[18] Steric hindrance between the rigid central parts induce alignment of the liquid crystal molecules (mesogens)

in one direction. The flexible segments bestow some mobility to mesogens because they are made of alkyl chains, which hinder crystallization to a certain degree. At low temperatures, mesogens are in the Cryst phase displaying positional order in three dimensions. Upon temperature increase, the system transitions into the SmA phase, where the positional order only in one dimension is preserved. Also, the molecules retain orientational order, i.e. the mesogens are oriented on average parallel to the layer normal and their arrangement is represented by a set of 2D liquid-like layers stacked on one another. At higher temperatures, in the nematic phase the positional order is lost but the orientational one is retained. In the Iso phase, the orientational order is completely lost. A newly developed spectrometer with a nearly Gaussian resolution function enabled us to perform the IXS measurements with unprecedented spectral contrast.[19] This led to the observation of clear inelastic spectral features down to an extremely low Q-value of 0.5 nm^{-1}. These measurements demonstrated for the first time explicit distinctions in the THz phononic response in different phases of the liquid crystal compound. Notably, investigation of the smectic *A* phase led us to discover the onset of a van der Waals-mediated non-hydrodynamic mode with an optical phononic behavior.

Cryst phase. The scattering geometry of the IXS experiment in the Cryst phase is shown in Fig.1a. The Cryst phase consisted of multiple crystalline domains with no discernible preferred orientation. The IXS spectra for Q-range of 1-5 nm^{-1} are shown in Fig.1b. Fig.1c displays sharp isolated diffraction peaks, which confirms that at T=25 ^{o}C the D7AOB sample is in the Cryst phase. Fig.1d shows the phononic dispersion curves determined from the best fit of the Damped Harmonic Oscillator (DHO) model to the IXS spectra (see **Methods**).

In Fig.1b two phononic branches, namely longitudinal acoustic (LA) and transverse acoustic (TA), can be clearly identified. The LA mode is the compression wave observable at Q=1 nm^{-1}, the lowest Q-value measured at T=25 ^{o}C, and is expected to emanate from the hydrodynamic long wavelength limit (E=0, Q=0). On the other hand, we argue that the presence of the TA mode (shear waves) in mesogens at THz frequencies is associated

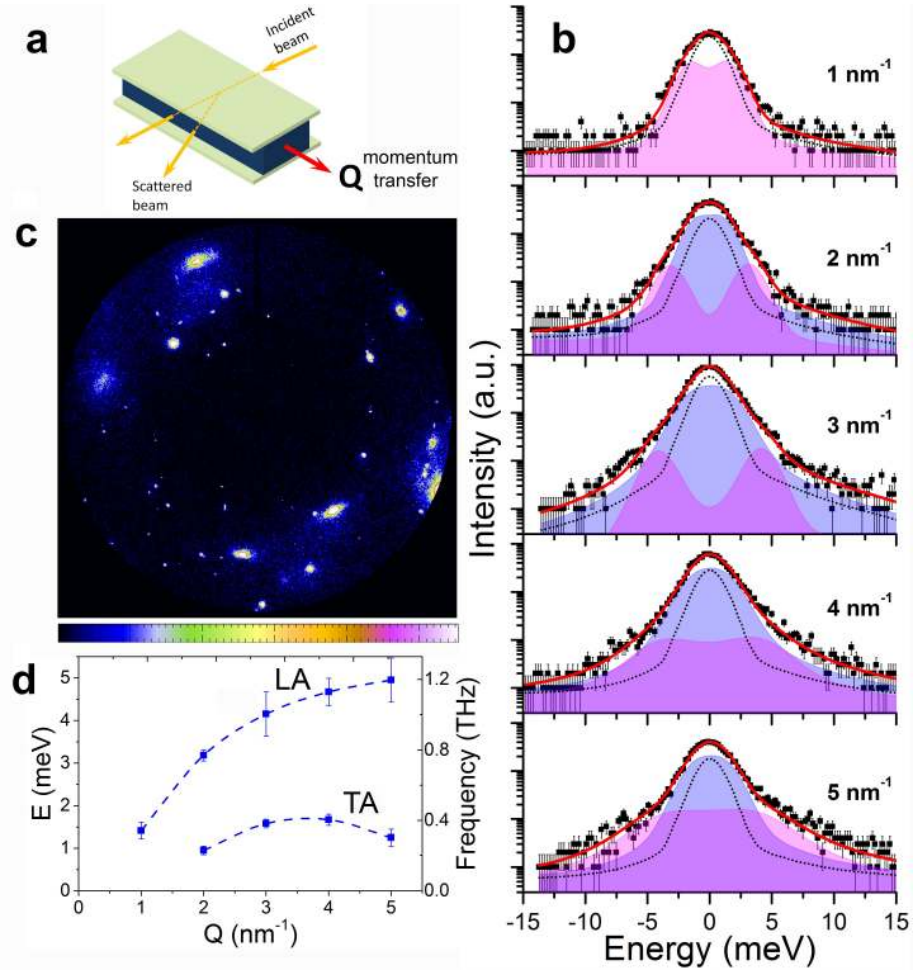

Figure 1: Phonon dynamics and sample structure in the Cryst phase. (a). Schematic of the scattering geometry of D7AOB at T=25 ^{o}C. The liquid crystal sample (dark blue) was confined between two glass plates (green). The scattering plane was parallel to the glass plates. (b). Inelastic x-ray scattering spectra of the sample. The experimental data are denoted by black squares together with error bars, the resolution function (black dotted line), and the best least square fit (red solid curves). Low- and high-frequency DHOs (see **Methods**) are denoted by the magenta and blue solid curves with the filled areas below them, respectively. The corresponding Q-values are shown in each plot. (c). Diffraction pattern of the sample. (d). LA and TA phononic branches.

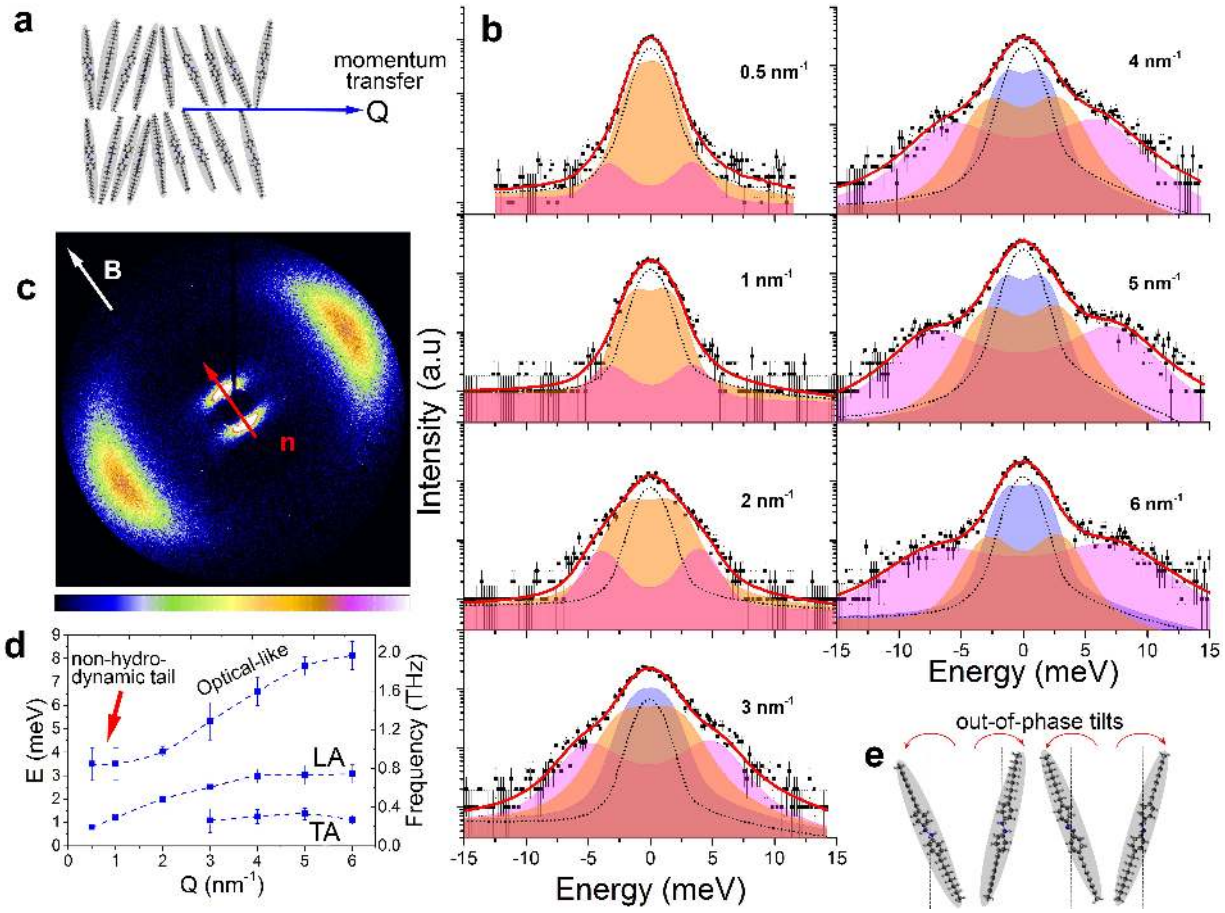

Figure 2: Phonon dynamics and sample structure in the SmA phase. (a). IXS scattering geometry. The scattering plane is perpendicular to the figure plane. (b). IXS spectra of D7AOB sample at T=48 ^{o}C. The experimental data (black squares) are reported together with the best fitting curve (red solid line) consisting of three DHO excitations: magenta, orange, and blue solid lines with the filled areas below them. The error bars are attributed to the signal-related statistical errors. The corresponding Q-values are shown to the right. (c). D7AOB x-ray diffraction pattern. White and red arrows denote the direction of the applied magnetic field **B** and the SmA layer normal **n**, respectively. (d). Dispersions of TA, LA and optical phononic modes. (e). The schematic representation of the out-of-phase mesogen tilts responsible for the emergence of the optical mode.

with rattling relaxation processes, which give rise to translational vibrational excitations activated at sub- and picosecond time scales. The energy and speed of sound of longitudinal phonons are always larger than that of the transverse phonons, which is reflected in higher amplitudes and speed of sound of longitudinal phonons, in particular. Therefore, we conveniently define the LA and TA modes as the ones lying at higher and lower excitation energies, respectively.

The TA mode is non-propagating at Q-values below 2 nm^{-1} exhibiting a propagation gap, also evidenced in other soft matter systems.[6,9] Rattling relaxation processes in soft matter systems originate from local interactions of neighboring molecules and, thus, are responsible for anharmonicity in a system.[20] These relaxation processes couple the propagation of LA and TA modes operating at the nanoscale in a way similar to the "cage" dynamics occurring in disordered materials such as liquids at the molecular level.[20,21]

SmA phase. Fig.2a displays the scattering geometry. Both the incident and the scattered beams lie within the plane parallel to the smectic layers. This ensures that the momentum transfer vector $\vec{Q}$ lies in the same plane and only probes the in-plane dynamics. Fig.2b shows IXS spectra covering an extended Q-range relevant for the detection of a non-hydrodynamic mode. In Fig.2c we present a diffraction pattern of the D7AOB sample in the SmA phase. The arcs at wide angle centered at Q=14.14 nm^{-1} with full width half maximum (FWHM) 4.46 nm^{-1} corresponds to an effective molecular width of 0.44 nm and a correlation length of 1.40 nm. This indicates that within the smectic planes, the mesogens are only sensitive to the positions of up to their third nearest neighbors. The arcs at small angle centered at Q=2.19 nm^{-1} with FWHM 0.09 nm^{-1} corresponds to an effective molecular length of 2.87 nm and a correlation length of 69.8 nm, which is limited by the resolution of our x-ray diffraction instrument. It has been previously shown,[18] that the smectic correlations as large as several thousand nm have been measured in well aligned samples (as this sample is) with high resolution instrument. The sharp inner peak also indicates the presence of long range positional order along the molecular long axis, which is ascribed to the formation of the

smectic layers. Furthermore, the 90^o difference in the azimuthal orientation of the wide and small angle peaks in the smectic phase confirms that the sample is in a SmA rather than SmC phase.[22]

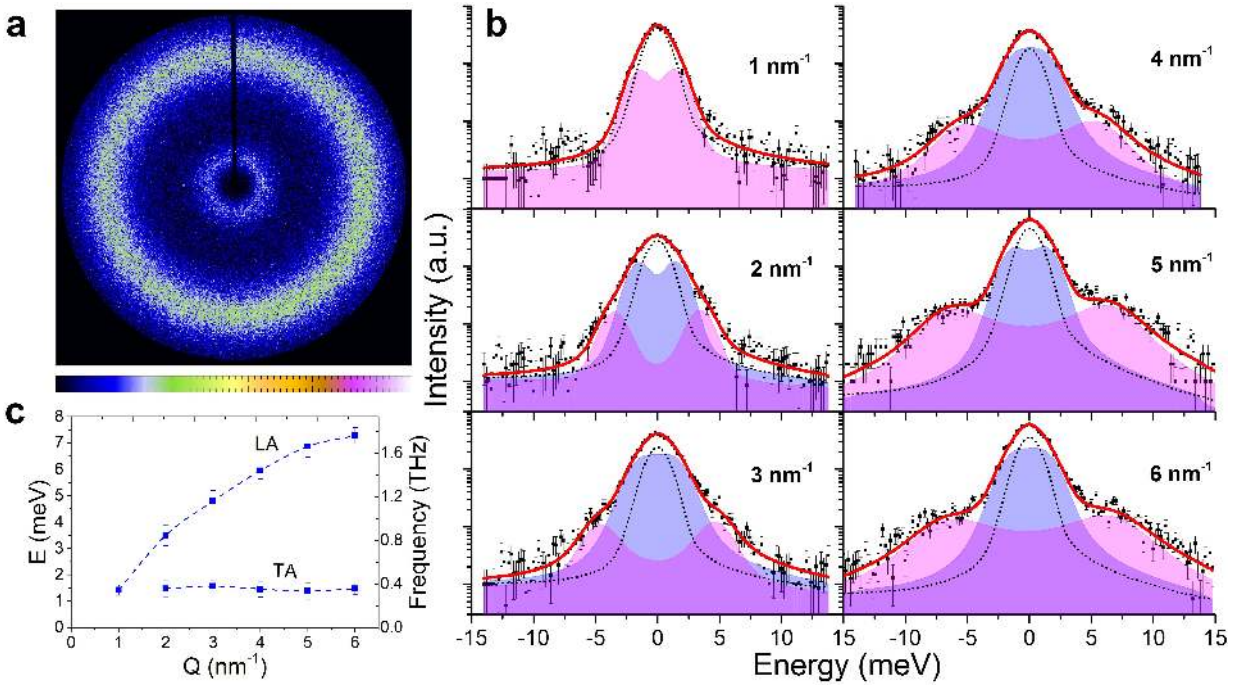

Figure 3: Phonon dynamics and sample structure in the Iso phase. (a). D7AOB diffraction pattern displays random molecular orientation. (b). IXS spectra of the sample at T=75 ^{o}C. The notation is the same as in Figure 1. (c). LA and TA phononic dispersions.

In the SmA phase, three phononic modes were observed from the IXS experiment (see Fig.2d). The justification for the chosen model is described in the Supplementary Information (SI). The conventional LA and TA excitations are similar to the ones in the Cryst phase. The LA mode in the SmA phase experiences the softening as compared to the Cryst phase, resembling other soft matter systems such as lipid membranes.[9] The TA mode in the SmA phase shows the increase of the propagation gap to Q=3 nm^{-1}, the behavior also discovered in lipids.[9] We caution that, an accurate determination of the propagation gap at mesogenic phase transitions is not possible due to current limits of the resolution function. Finally, we note that, the TA mode is distinctly different from the SmA "second sound" hydrodynamic mode. The "second sound" mode involves only smectic layer displacements and is diffusive

along the SmA symmetry directions, including the in-plane direction probed by the IXS measurements.

In addition to the LA and TA modes, we observed optical-like excitations at elevated energies. This optical phononic branch exhibits a non-hydrodynamic "tail" (no dispersion, see Fig.2d) in the long wavelength limit. This phenomenon can be understood in the context of mesogenic movements in the SmA phase. The SmA phase is characterized by two types of molecular motions: translational vibrational modes and mesogenic tilts where adjacent mesogens swing around one another. The former gives rise to acoustic modes, while the latter governs the optical one. Indeed, in the tilt motion, each mesogen keeps a nearly fixed position at subpicosecond and picosecond time scales, while periodically tilting back and forth around its center of mass (see Fig.2e). Thus, these out-of-phase movements of mesogens exhibit non-hydrodynamic dispersion (see Fig.2d) toward the limit of infinitesimal Q's, where they give rise to an optical phononic mode. Similar displacement patterns were previously observed in the form of overtones of Raman lines in various mesogenic systems.[23–26] In particular, ultra-low Raman active modes of the liquid crystal compound octylcyanobiphenyl (8CB) in the SmA phase were detected within the range of 10-20 cm^{-1} (1.2-2.4 meV).[26] 8CB, an asymmetric polar molecule with rigid head and one flexible tail, resembles the D7AOB structure.[18] These tilt modes in 8CB were assigned to inter-molecular motions being also called librations or "breathing modes", which retain an optical phononic character.[27] Importantly, we also observed a hybridization gap between the optical-like and the LA mode,[28,29] which appears due to the avoided crossing (also called the anti-crossing) of two phononic bands of the same symmetry that occurs withing $\sim$ 2.8-3.4 meV energy range (see Fig.2d). Finally, we note that the optic mode is consistent with the measurements of the thermal diffusivity in the nematic and smectic *A* phases, which indicated the existence of nanoscale-THz modes.[30]

Iso phase. In Fig.3a we show the diffraction pattern of the sample in the Iso-phase. X-ray diffraction shows two concentric rings centered at Q= 3.10 nm^{-1} and 13.68 $\pm$0.1

nm^{-1}, with corresponding FWHM of 2.12 nm^{-1} and 5.20 ± 1 nm^{-1}, which indicate random mesogenic orientation. The ring centered at Q= 3.10 nm^{-1} corresponds to the effective molecular length of 2.03 nm, with a correlation length of 2.96 nm. The ring centered at Q= 13.68 nm^{-1} corresponds to the effective molecular width of 0.46 nm, which is typical of hydrocarbon chains.[22] IXS spectra and phononic dispersion relations in the Iso-phase are presented in Fig.3b and Fig.3c, respectively.

Mesogens in the Iso phase can slide over one another accompanied with hindered rotations. Translational-rotational motions are tightly coupled resulting in one longitudinal mode (LA, see Fig.3c). Therefore, the LA mode in the Iso phase can be considered as a superposition of the longitudinal optical-like mode and the LA one in the SmA phase. In the Iso phase, mesogens' centers of masses are not ordered and not fixed at the picosecond time scale, which leads to the absence of a non-hydrodynamic (localized) "tail" of the low-Q dispersion of the longitudinal vibrations. Alike, in the Cryst phase, the mesogens may support independent small amplitude tilt-like motions. Nevertheless, it would be hard to observe such out-of-phase displacements as a collective effect, that could generate optical phononic excitations. Longitudinal translations in the Iso phase (LA mode in Fig.3c) are less energetic than their optical counterparts in the SmA phase (optical-like mode in Fig.2d) because rotations in the Iso phase are considerably hindered. At the same time, the LA mode is more energetic in the Iso phase (Fig.3c) than in the SmA phase (Fig.2d) due to coupling with rotational motions. A translational-rotational mode coupling was also found in highly anisotropic molecular systems as phenyl-salicylate (Salol),[31,32] as well as in the Iso phase of the liquid crystals *p*-methoxybenzylidene-*n*-butylaniline (MBBA), triphenylphosphite (TPP), 4'-pentyl-4-cyanobiphenyl (5CB) and their mixtures.[33,34] It explains why, in the Iso phase, high frequency dispersions merge into a single branch rather than splitting as in the SmA phase. Therefore, the merging of the dispersion curves at intermediate and high Q's leads to a shift of the longitudinal branch towards higher energies (phononic hardening, see Fig.3c) than in the Cryst or SmA phases. In other words, the presence of LA excita-

tions at elevated energies manifests the phononic hardening due to random close-packing and translational-rotational mode coupling of mesogens.

The TA phononic branch in the Iso phase is non-dispersing indicating its strong localization. The propagation gap is observed at lower Q-value as compared to the SmA phase. The measured dynamical behavior of the LA and TA modes in the Iso phase is consistent with the recently observed hidden long-range solid-like properties of the isotropic phase.[35]

Discussion. The Q-dependence of both acoustic and optical phononic modes in liquid crystals at THz frequencies has never been measured before since techniques such as Raman spectrocopy are inherently unable to probe it. Moreover, no optical phononic modes have been observed in similar soft matter materials such as lipid membranes.[36,37] Only recently, low-energy TA modes were experimentally observed in DPPC lipid membranes using IXS,[9] but the optical phononic modes in such systems remained elusive. Therefore, the detected optical phononic excitations in D7AOB (see Fig.2d) with IXS signifies the practical importance of this system for future optomechanical applications. Mesogens such as cyanobiphenyls (CBs) are infrared-active materials within the frequency range of 0.3-15 THz (1.2-62 meV).[38,39] We have shown that the van der Waals-mediated non-hydrodynamic "tail" of the optical phononic mode, which implies non-vanishing damping in the large coupling limit, in the SmA phase converges to $\sim$3.5 meV (0.8 THz, see Fig.2d) matching the wavelength absorption band of CBs.

Recently, a practical realization of a cavity-optomechanics concept based on the interaction between light and mechanical objects on low-energy scales has been demonstrated in phononic crystal waveguides at GHz-frequencies.[40] The interaction of light with localized optical phonons resulted in a tunable delay and filter for microwave-over-optical signals as well as provided the possibility for performing coherent signal processing.[40] Other phenomena employing the cavity-optomechanical principle at MHz-GHz frequencies have been studied too.[41,42]

In the case of THz light-phonon interactions, similar concepts can be realized as well. For example, for liquid crystals, the electric field of the infrared light may tilt in-phase mesogens in the direction of the field, and each out-of-phase mesogens in the opposite direction, leading to the propagation of an optical phononic excitation. For such a practical realization a deeper understanding of phonon behavior at THz-scale is, therefore, vital. We believe that soft matter materials such as liquid crystals, whose morphology and phase behavior can easily be manipulated as compared to their solid-state counterparts, are ideal candidates for optomechanical applications. There are very few techniques capable of probing THz phononics with Q-dependence. IXS is ideally suited for such studies. The IXS technique is virtually free from "inherent" kinematic limitations, however, ω values accessible by this method are still restricted for ultralow values. These limitations are caused by the relatively broad resolution linewidth and, perhaps, more importantly, due to the poor spectral contrast attainable with the Lorentzian resolution shape in most current high-resolution IXS facilities. To mitigate these limitations, we took advantage of the new IXS beamline 10-ID at the National Synchrotron Light Source II, Brookhaven National Laboratory, which offers an energy resolution function shape with a nearly Gaussian profile. The high spectral contrast of the resolution function is the key factor in determining the changes in the slope of the dominant central peak's tails. The change in the central peak slope corresponds to the emergence of an additional mode in the spectrum. Noteworthy, the intensity of the TA mode is comparable with the intensity of the dominant central peak. As follows from the Figs. 1d, 2d, and 3c, the TA modes are located within 1-2 meV excitation energy range, which is comparable with the FWHM of the resolution function ($\sim$2 meV). Clearly, the TA modes do not lie within the resolution function making it possible to unambiguously resolve them. The much improved resolution profile also enabled the observation of a spectral mode in the partially disordered system exhibiting a non-hydrodynamic behavior and becoming localized at very low Q-values.

One may expect a new technological breakthrough for liquid crystals thanks to, for instance, the so-called topological defects, which are being exploited to produce structures with extraordinary properties.[43–45] In this work, we showed that modulating the amount of structural disorder through the access to different mesogenic phases in a narrow temperature range can lead to the emergence a variety of phononic effects. For the first time, we demonstrated that liquid crystals are able to support both acoustic and optical phononic excitations propagating down to the nanoscale. Thus, we believe that mesogenic systems could be ideal candidates for novel phononic and optomechanical applications to achieve new functionalities in the nanometer-terahertz window.

Methods

IXS measurements. IXS spectra were measured at the 10-ID beamline of the National Synchrotron Light Source II, Brookhaven National Laboratory. Measurements were performed at an incident photon energy of 9.13 keV. The energy resolution function had nearly a Gaussian profile with ∼2 meV full width at half maximum. The incident X-ray beam was focused on the sample to within a 10×10 μm^2 focal spot. The incident flux was ∼2×10^9 photons/sec. The D7AOB sample was contained between two glass plates (2×25 mm) with a 50 micron Mylar spacer. The sample thickness of 50 microns was chosen to minimize surface effects; a sample of this thickness contains several thousand smectic layers whereas surface effects in smectic liquid crystals, away from a phase transition, typically extend less than a few smectic layers.[46] The glass plates were coated with Quilon H (Sigma-Aldrich) for hometropic alignment (i.e., mesogens orient perpendicular to the glass plates in the SmA phase). The sample cell was then placed inside the Linkam hotstage (LTS420) linked to temperature controller with ±0.1 ^{o}C temperature stability. The scattering intensity was collected in the horizontal plane, with the lateral planes of the D7AOB sample parallel to the plane of scattering, hence, only in-plane dynamics was probed. A single IXS scan included 151 energy points with an acquisition time of 90 seconds per point. In fitting procedure we used the model consisting of multiple DHOs excitations plus a $\delta\omega$ central peak. The resulting fitting lineshapes are

obtained through the convolution with the instrumental resolution function. The sample was translated across the beam at each scan to avoid beam damage.

X-ray diffraction measurements. X-ray diffraction data were obtained from a sample of D7AOB filled into 1 mm flame sealed quartz capillary. The sample capillary was placed inside a Linkam HFS350X-CAP hotstage with ± 0.1 ^{o}C temperature stability, for controlled heating and cooling. The D7AOB sample was aligned in the nematic phase by means of a 2.5 kG magnetic field produced by a pair of samarium cobalt rare-earth magnets mounted on opposite sides of the sample capillary. This alignment persisted into the SmA phase during cooling. The measurements were performed using a Rigaku Screen Machine with microfocus sealed copper x-ray tube with a copper anode (λ =1.54 Å). Images were collected using a Mercury 3-CCD detector with resolution 1024×1024 pixels and pixel size of 73.2×73.2 μm^2 placed 78.5 mm from the sample. The 2D x-ray patterns were analyzed using the software FIT2D after subtracting the background measured with an empty capillary in the sample position. The data were calibrated against silver behenate standards traceable to the National Institute of Standards and Technology.

Acknowledgement

We thank Peter S. Pershan for fruitful discussions. We acknowledge the US-Ireland R&D Partnership program of the National Science Foundation award No. DMR- 1410649. The work at the National Synchrotron Light Source-II, Brookhaven National Laboratory, was supported by the U. S. Department of Energy, Office of Science, Office of Basic Energy Sciences, under Contract No. DE-SC0012704.

References

(1) Maldovan, M. *Nature* **2013**, *503*, 209–217.

(2) Schneider, D.; Gomopoulos, N.; Koh, C. Y.; Papadopoulos, P.; Kremer, F.; L., T. E.; Fytas, G. *Nat. Mater.* **2016**, *15*, 1079–1083.

(3) Mousavi, S. H.; Khanikaev, A. B.; Wang, Z. *Nat. Commun.* **2015**, *6*, 8682.

(4) Yu, S.-Y.; Sun, X.-C.; Ni, X.; Wang, Q.; Yan, X.-J.; He, C.; Liu, X.-J.; Feng, L.; Lu, M.-H.; Chen, Y.-F. *Nat. Mater.* **2016**, *15*, 1243–1247.

(5) Yudistira, D.; Boes, A.; Graczykowski, B.; Alzina, F.; Yeo, L. Y.; Torres, C. M. S.; Mitchell, A. *Phys. Rev. B* **2016**, *94*, 094304.

(6) Bolmatov, D.; Zhernenkov, M.; Zav'yalov, D.; Stoupin, S.; Cunsolo, A.; Cai, Y. Q. *Sci. Rep.* **2016**, *6(15)*, 19469.

(7) Xiao, M.; Chen, W.-J.; He, W.-H.; Chan, C. T. *Nat. Phys.* **2015**, *11*, 920–924.

(8) Yang, Z.; Gao, F.; Shi, X.; Lin, X.; Gao, Z.; Chong, Y.; Zhang, B. *Phys. Rev. Lett.* **2015**, *114*, 114301.

(9) Zhernenkov, M.; Bolmatov, D.; Soloviov, D.; Zhernenkov, K.; Toperverg, B. P.; Cunsolo, A.; Bosak, A.; Cai, Y. Q. *Nat. Commun.* **2016**, *7*, 11575.

(10) Ma, G.; Sheng, P. *Sci. Adv.* **2016**, *2*, e1501595.

(11) Ma, G.; Fu, C.; Wang, G.; del Hougne, P.; Christensen, J.; Lai, Y.; Sheng, P. *Nat. Commun.* **2016**, *7*, 13536.

(12) Elton, D. C.; Fernández-Serra, M. *Nat. Commun.* **2016**, *7*, 10193.

(13) Sinn, H.; Glorieux, B.; Hennet, L.; Alatas, A.; Hu, M.; Alp, E. E.; Bermejo, F. J.; Price, D. L.; Saboungi, M.-L. *Science* **2003**, *299*, 5615.

(14) Bencivenga, F.; Cunsolo, A. *J. Chem. Phys.* **2012**, *136*, 114508.

(15) Bolmatov, D.; Zhernenkov, M.; Zav'yalov, D.; Stoupin, S.; Cai, Y. Q.; Cunsolo, A. *J. Phys. Chem. Lett.* **2015**, *6(15)*, 3048–3053.

(16) Balucani, U.; Zoppi, M. *Dynamics of the Liquid State*; Clarendon Press: Oxford, 1994.

(17) Cunsolo, A. *Appl. Sci.* **2016**, *6(3)*, 64.

(18) Primak, A.; Fisch, M.; Kumar, S. *Phys. Rev. E* **2002**, *66*, 051707.

(19) Cai, Y. Q.; Coburn, D. S.; Cunsolo, A.; Keister, J. W.; Honnicke, M. G.; Huang, X. R.; Kodituwakku, C. N.; Stetsko, Y.; Suvorov, A.; Hiraoka, N.; Tsuei, K. D.; Wille, H. C. *J. of Phys.: Conf. Series* **2013**, *425*, 202001.

(20) Bolmatov, D.; Zav'yalov, D.; Zhernenkov, M.; Musaev, E. T.; Cai, Y. Q. *Ann. Phys.* **2015**, *363*, 221–242.

(21) Bolmatov, D.; Musaev, E. D.; Trachenko, K. *Sci. Rep.* **2013**, *3*, 2794.

(22) Kumar, S. *Liquid Crystals: Experimental Study of Physical Properties and Phase Transitions*; Cambridge University Press: Cambridge, 2001.

(23) Amer, N. M.; Shen, Y. R. *Solid State Commun.* **1973**, *12*, 263–265.

(24) Dvorjetski, D.; Volterra, V.; Wiener-Avnear, E. *Phys. Rev. A* **1975**, *12*, 681.

(25) Fontana, M. P.; Bini, S. *Phys. Rev. A* **1976**, *14*, 1555.

(26) Hsueh, H. C.; Vass, H.; Pu, F. N.; Clark, S. J.; Poon, W. C. K.; Crain, J. *Europhys. Lett.* **1997**, *38(2)*, 107–112.

(27) Tuschel, D. *Spectroscopy* **2015**, *30(3)*, 14–29.

(28) Still, T.; Cheng, W.; Retsch, M.; Sainidou, R.; Wang, J.; Jonas, U.; Stefanou, N.; Fytas, G. *Phys. Rev. Lett.* **2008**, *100*, 194301.

(29) Alonso-Redondo, E.; Schmitt, M.; Urbach, Z.; Hui, C. M.; Sainidou, R.; Rembert, P.; Matyjaszewski, K.; Bockstaller, M. R.; Fytas, G. *Nat. Commun.* **2015**, *6*, 8309.

(30) Urbach, W.; Hervet, H.; Rondelez, F. *Mol. Cryst. Liq. Cryst.* **1978**, *46*, 209–221.

(31) Yang, Y.; Nelson, K. A. *J. Chem. Phys.* **1995**, *103*, 18.

(32) Zhang, H. P.; Brodin, A.; Barshilia, H. C.; Shen, G. Q.; Cummins, H. Z.; Pick, R. M. *Phys. Rev. E* **2004**, *70*, 011502.

(33) Shibata, T.; Matsuoka, T.; Koda, S.; Nomura, H. *J. Chem. Phys.* **1998**, *109*, 2038.

(34) Matsuoka, T.; Mizoguchi, Y.; Koda, S.; Onoda-Yamamuro, N.; Ogawa, H.; Nomura, H. *J. Mol. Liq.* **2005**, *119*, 107–111.

(35) Kahl, P.; Baroni, P.; Noirez, L. *Phys. Rev. E* **2013**, *88*, 050501(R).

(36) Chen, S. H.; Liao, C. Y.; Huang, H. W.; Weiss, T. M.; Bellisent-Funel, M. C.; Sette, F. *Phys. Rev. Let.* **2001**, *86*, 740–743.

(37) Chen, P. J.; Liu, Y.; Weiss, T. M.; Huang, H. W.; Sinn, H.; Alp, E. E.; Alatas, A.; Said, A.; Chen, S. H. *Biophys. Chem.* **2003**, *105*, 721–741.

(38) Vieweg, N.; Fischer, B. M.; Reuter, M.; Kula, P.; Dabrowski, R.; Celik, M. A.; Frenking, G.; Koch, M.; Jepsen, P. E. *Opt. Express* **2012**, *20*, 28249–28256.

(39) Vieweg, N.; Celik, M. A.; Zakel, S.; Gupta, V.; Frenking, G.; Koch, M. *J. Infrared Milli. Terahz. Waves* **2014**, *35*, 478.

(40) Fang, K.; Matheny, M. H.; Luan, X.; Painter, O. *Nat. Photon.* **2016**, *10*, 489–496.

(41) Shen, Z.; Zhang, Y. L.; Chen, Y.; Zou, C. L.; Xiao, Y. F.; Zou, X. B.; Sun, F. W.; Guo, G. C.; Dong, C. H. *Nat. Photon.* **2016**, *10*, 657–661.

(42) Riedinger, R.; Hong, S.; Norte, R. A.; Slater, J. A.; Shang, J.; Krause, A. G.; Anant, V.; Aspelmeyer, M.; Gröblacher, S. *Nature* **2016**, *530*, 313–316.

(43) Wang, X.; Kim, Y. K.; Bukusoglu, E.; Zhang, B.; Miller, D. S.; Abbott, N. L. *Phys. Rev. Lett.* **2016**, *116*, 147801.

(44) Zhu, C.; Wang, C.; Young, A.; Liu, F.; Gunkel, I.; Chen, D.; Walba, D.; Maclennan, J.; Clark, N.; Hexemer, A. *Nano Lett.* **2015**, *15(5)*, 3420–3424.

(45) Wang, X.; Miller, D. S.; Bukusoglu, E.; de Pablo, J. J.; Abbott, N. L. *Nat. Mater.* **2016**, *15*, 106–112.

(46) Heinekamp, S.; Pelcovits, R. A.; Fontes, E.; Chen, E. Y.; Pindak, R.; Meyer, R. B. *Phys. Rev. Lett.* **1984**, *52*, 1017.

Graphical TOC Entry